ChemPubSoc Europe

DOI: 10.1002/cphc.202000041

CHEMPHYSCHEM Articles

IRMPD Spectra of Protonated Hydroxybenzaldehydes: Evidence of Torsional Barriers in Carboxonium Ions

Barbara Chiavarino,*[a] Otto Dopfer,[b] Maria Elisa Crestoni,[a] Davide Corinti,[a] Philippe Maître,[c] and Simonetta Fornarini[a]

Protonation at the formyl oxygen atom of benzaldehydes leading to the formation of carboxonium ions yields two distinct isomers, depending on the relative orientation of the proton either *cis* or *trans* with respect to the hydrogen atom on the adjacent carbon. In this context, the IR multiple photon dissociation (IRMPD) spectra of protonated *ortho*, *meta*, and *para*-hydroxybenzaldehydes (**OH–BZH$^+$**), delivered into the gas phase by electrospray ionization of hydro-alcoholic solutions, are reported in the 3200–3700 cm^{-1} spectral range. This range is characteristic of O–H stretching modes and thus able to differentiate *cis* and *trans* carboxonium isomers. Comparison between IRMPD spectra and DFT calculations at the B3LYP/6-311++G(2df2p) level suggests that for both ***p*-OH–BZH$^+$** and ***m*-OH–BZH$^+$** only *cis* conformers are present in the ion population analyzed. For ***o*-OH–BZH$^+$**, IRMPD spectroscopy points to a mixture comprising one *trans* and more than one *cis* conformers. The energy barrier for *cis–trans* isomerization calculated for each **OH–BZH$^+$** isomer is a measure of the degree of π-electron delocalization. Furthermore, IRMPD spectra of ***p*-OH–BZH$^+$**, ***m*-OH–BZH$^+$** and protonated phenol (this last used as reference) were recorded also in the fingerprint range. Both the observed C–O and O–H stretching vibrations appear to be a measure of π-electron delocalization in the ions.

1. Introduction

The elucidation of the intrinsic characteristics, such as structure, reactivity, and energetics of ions produced by protonation of simple aromatic molecules, like benzene and its (mono) substituted derivatives, is of crucial interest in the field of physical, organic and biological chemistry. When protonation occurs at the aromatic ring, an arenium ion is obtained, key intermediate in electrophilic aromatic substitution reactions.[1] In some peculiar examples such as aniline, phenol and fluorobenzene, vibrational spectroscopy of the gaseous ions has shown that both aromatic ring and substituent undergo protonation.[2]

Protonation at the substituent is largely favored in the presence of highly basic units such as an amino group or when the ring substituent combines an electron-withdrawing effect with significant basicity, such as the carbonyl group of an aromatic aldehyde or ketone.[3] The basicity of aromatic aldehydes is a topic of ongoing interest.[4] Protonation of benzaldehyde is directed onto oxygen yielding a carboxonium ion.[5] These ions, first noted in the work of Meerwein,[6] are stabilized by conjugation due to the oxygen atom bound to the positively charged carbon when compared with the corresponding alkylaryl cations.[7] They display dual facets as oxonium and carbenium ion, with prevailing oxonium character (Scheme 1).

In substituted protonated benzaldehydes, however, the prevalence of the carbenium or oxonium character depends on the features and relative position of any other ring substituent, as highlighted by NMR spectroscopy and theoretical studies.[8]

The present contribution follows along the lines of the continuing interest in the structural characterization of protonated aromatic compounds by isolating them in the gas phase and sampling by IR spectroscopy.[9] Herein, IR multiple photon dissociation (IRMPD) spectra and quantum chemical calculations are reported for gaseous protonated hydroxybenzaldehydes. Recent interest in these compounds arises from the fact that, by analogy to other phenolic compounds, hydroxybenzaldehydes generated during the pretreatment of lignocellulose biomass have been identified as key inhibitors in biomass hydrolysates, which considerably prevent microbial growth and decrease the fermentation rate.[10] In particular, in a study aimed at finding a structure-inhibitory activity relationship of carbonyl compounds in alcoholic fermentation, it was observed that *para*-hydroxybenzaldehyde increased the final ethanol yields.[11]

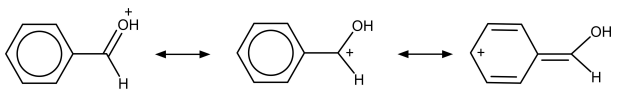

Scheme 1. Structure of the oxonium, hydroxycarbenium, and ring carbenium ions.

[a] Prof. B. Chiavarino, Prof. M. E. Crestoni, Dr. D. Corinti, Prof. S. Fornarini
Dipartimento di Chimica e Tecnologie del Farmaco
Università di Roma "La Sapienza"
P.le A. Moro 5, 00185 Roma, Italy
E-mail: barbara.chiavarino@uniroma1.it
[b] Prof. O. Dopfer
Institut für Optik und Atomare Physik
Technische Universität Berlin
Hardenbergstrasse 36, 10623 Berlin, Germany
[c] Dr. P. Maître
Institut de Chimie Physique, UMR8000, CNRS
Université Paris-Saclay, 91405, Orsay, France

Supporting information for this article is available on the WWW under https://doi.org/10.1002/cphc.202000041

Another recent study has reported that *ortho*-hydroxybenzaldehyde has been found responsible for 15-20-fold higher inhibition of the alcoholic fermentation by saccharomyces cerevisiae, as compared to *meta* and *para* isomers.[12] The high inhibitory activity of *ortho*-hydroxybenzaldehyde was attributed to its peculiar capacity of forming an intramolecular hydrogen bond (H-bond) between the oxygen atom of the formyl group and the hydrogen atom of the hydroxyl substituent, which can improve its cell membrane permeability and toxicity. Analogously, the proximity of the two substituents in *ortho*-hydroxybenzaldehyde is expected to play an important role in the protonation reaction.

The aim of the present study was to strengthen and extend the previous evidence about the structure of protonated benzaldehyde obtained by IR(M)PD spectroscopy in both the fingerprint[13] and OH stretching ranges,[14] and by electronic photodissociation in the visible range.[15] To this end, we envisioned to relate the characteristic OH stretching mode of the protonated carbonyl group with another OH group directly attached to the phenyl ring. Previous studies have evidenced that the exclusive protonation site of gaseous benzaldehyde is the oxygen atom, as also observed in condensed phase.[16] Similar to protonated aliphatic aldehydes, protonation at the formyl oxygen atom of (hydroxy)benzaldehydes leads to the formation of carboxonium ions in two isomeric forms, depending on the relative orientation of the incoming proton, either *cis* or *trans* with respect to the hydrogen atom on the adjacent carbon (see Figure 1). In this context, the 3200–3700 cm^{-1} spectral range should allow to distinguish *cis* and *trans* carboxonium isomers by their characteristic OH stretching frequency.

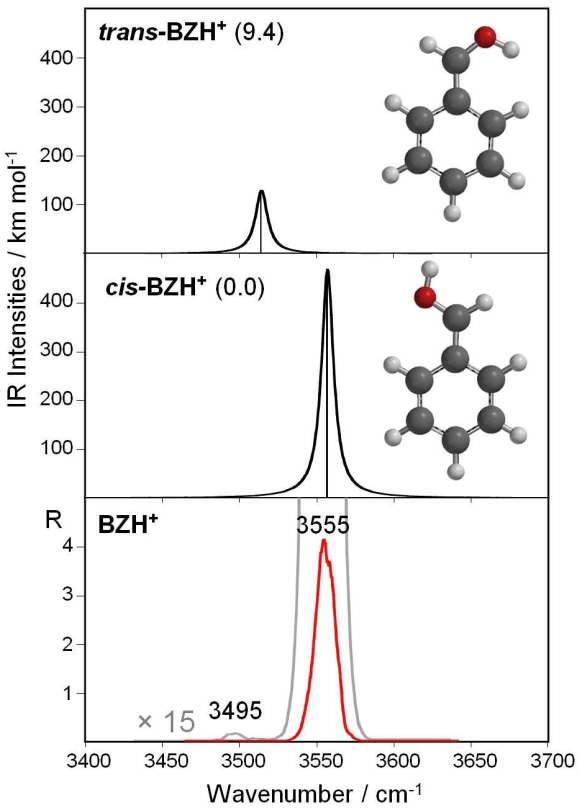

Figure 1. Experimental IRMPD spectrum of protonated benzaldehyde (**BZH$^+$**, bottom) in the OH stretching range compared with the IR spectra of the two carboxonium isomers computed at the B3LYP/6-311++G (2df2p) level. Relative free energy values are given in parenthesis (kJ/mol).

2. Results and Discussion

2.1. Protonated Benzaldehyde

Initially, the IRMPD spectrum of protonated benzaldehyde (**BZH$^+$**) was newly recorded to check consistency with our previously reported results.[13,14] In fact, both the present experimental apparatus and the way to generate ions differ from the ones employed in previous studies. In particular, in the present study gaseous ions were generated by electrospray ionization (ESI), a milder ionization method than the previously used exothermic proton transfer in the gas phase.

The IRMPD spectrum of **BZH$^+$** is reported in Figure 1 together with the newly calculated IR spectra of ***cis*-BZH$^+$** and ***trans*-BZH$^+$**. Confirming previous calculations,[13,14] the *cis* rotamer was found 9.4 kJ/mol more stable than the *trans* rotamer. The interconversion free energy barrier from *cis* to *trans* conformation by rotation of the OH group around the C–O bond is 65.2 kJ/mol, as shown in Figure S1 (in the Supporting information) where the potential energy surface (PES) of the isomerization path of **BZH$^+$** is reported.

The presently reported IRMPD spectrum of **BZH$^+$** in the OH stretching range exhibits only a single band at 3555 cm^{-1} corresponding to the O–H stretching mode of ***cis*-BZH$^+$**, as evidenced by calculated spectra for the two isomers. Only when both laser power and irradiation time were increased by a factor of 4, causing saturation and complete depletion of the precursor ion signal at the frequency of 3555 cm^{-1}, a second small band appeared at 3495 cm^{-1}. This feature, relatively more intense in the previously reported experiment, may suggest the presence of a minute amount of the higher energy ***trans*-BZH$^+$** isomer.[14]

2.2. Protonated *p*-Hydroxybenzaldehyde

The focus of this paper is to understand whether the presence of a hydroxyl group on the ring will influence the configuration of the carboxonium ion. In protonated *p*-hydroxybenzaldehyde (***p*-OH–BZH$^+$**), the *cis* and *trans* carboxonium isomers may present a different orientation of the phenolic OH group, giving rise to a total of four possible rotamers. To make a distinction, *syn* is used to indicate that both O-bound hydrogen atoms show a clockwise orientation, whereas *anti* means that one of the two displays an anticlockwise orientation. Figure 2 shows the four optimized ***p*-OH–BZH$^+$** isomers together with their relative energies at 298 K.

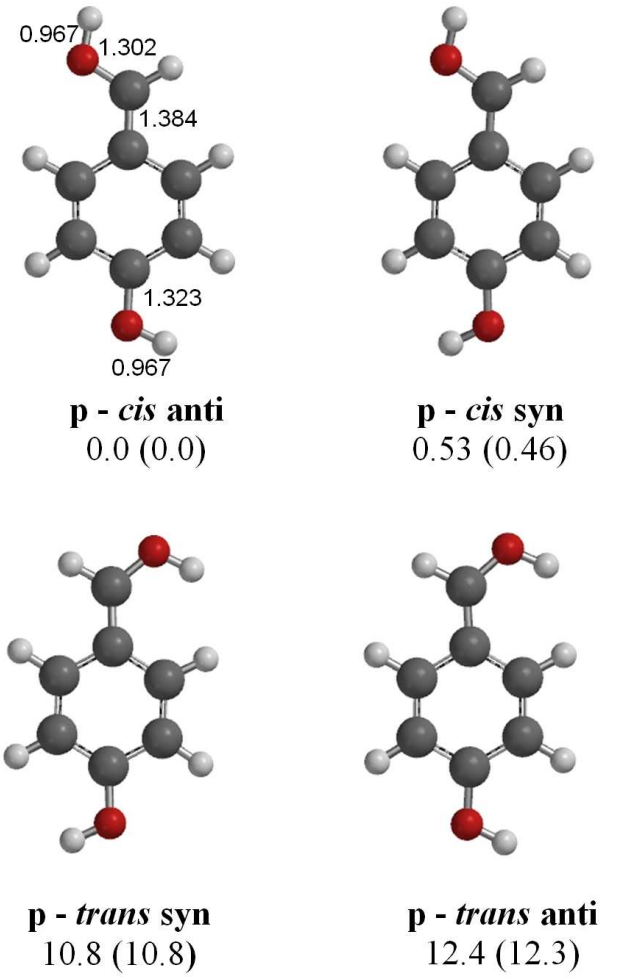

Figure 2. Optimized geometries of ***p*-OH–BZH$^+$** formed by protonation at the formyl oxygen atom. Relative enthalpy and free energy (in parentheses) values (kJ/mol) at 298 K are computed at the B3LYP/6-311++G(2df2p) level.

As observed for **BZH$^+$**, all optimized geometries in Figure 2 are planar to maximize π conjugation. Moreover, the two *cis* conformers with comparable energy (0.46 kJ/mol difference in free energy) are more stable than the two *trans* conformers by approximately 11 kJ/mol. The global minimum corresponds to the **p-*cis* anti** conformer while **p-*trans* anti** is the least stable of the four carboxonium ions, lying at 12.3 kJ/mol relative energy. Interestingly, the presence of the *para*-OH group facilitates *cis/trans* isomerization. The computed energy barrier for the interconversion from **p-*cis* anti** to **p-*trans* syn** is 51.2 kJ/mol, i.e., 14 kJ/mol less that the torsional *cis-trans* barrier calculated for **BZH$^+$**. The energy profile for the interconversion between all carboxonium isomers of ***p*-OH–BZH$^+$** is reported in Figure S2. This result is in agreement with previous theoretical and experimental studies reporting that the presence of electron-donor substituents in *para*-substituted benzaldehydes improves the conjugative interaction with the aryl ring via the π-electron system and, consequently, decreases the double bond character of the C–OH protonated formyl group due to a diminished weight of the oxonium description (e.g. resonance structures (**a**) versus resonance structure (**b**) in Figure 3).[8a,c] The relatively high energy of the transition state for *syn/anti* isomerization, via rotation of the phenolic OH group (34.9 and 34.5 kJ/mol for the *cis* and *trans* species, respectively, Figure S2), is a further confirmation for extensive π conjugation, as depicted in the resonance structures (**a**) in Figure 3.

Moreover, considering that OH is a typical *ortho/para* directing group, while CHO is *meta* directing, it is plausible that protonation of *p*-hydroxybenzaldehyde may also occur on a ring carbon atom, which is both *meta* to the formyl and *ortho* to the OH substituent. However, this carbenium isomer (***p*-OH–C_6H_5–CHO$^+$**) is found to be much higher in energy relative to the most stable species (by more than 100 kJ/mol). The optimized geometry together with its calculated IR spectrum computed at the B3LYP/6-311++G(2df2p) level are reported in Figure S3 together with the experimental IRMPD spectrum of ***p*-OH–BZH$^+$**.

In the O–H stretching range, ***p*-OH–BZH$^+$** yields only one photofragment at *m/z* 95 (by loss of CO), formally corresponding to protonated phenol. This photofragmentation pathway is common to all protonated hydroxybenzaldehydes analyzed in the O–H spectral range and the same *m/z* 95 fragment was obtained also in collision-induced dissociation (CID) experiments. The IRMPD spectrum of ***p*-OH–BZH$^+$** recorded in the 3400–3700 cm^{-1} range is compared in Figure 4 with the spectra calculated for the low-energy isomers already shown in Figure 2. The experimental spectrum shows only a single O–H stretch band centered at 3576 cm^{-1}, in excellent agreement with the spectra calculated for the ***cis*** conformers. In fact, the IR spectra of the **p-*cis*** conformers display only one feature centered at 3576 cm^{-1} because of the - overlap of the coupled HCO–H (OH_{fo}) and phenolic O–H stretching vibrations (OH_{ph}) (both at 3576 cm^{-1} for **p-*cis* anti**, 3576 and 3585 cm^{-1} for **p-*cis* syn**). In the calculated spectra of the two **p-*trans*** rotamers, the two vibrational modes are distinct and separated by ca. 40 cm^{-1}. The OH_{fo} stretch moves to lower frequency, at 3540 cm^{-1}. In spite of the reduced energy barrier for *cis/trans* interconversion, the lack of any signal around 3540 cm^{-1} is clear evidence that only the low energy **p-*cis*** conformers are present in the ***p*-OH–BZH$^+$** ion population, as already observed for **BZH$^+$**. Finally, the OH_{ph} stretching mode calculated at 3540 cm^{-1} for ring-protonated **p-OH–C_6H_5–CHO$^+$** is missing in

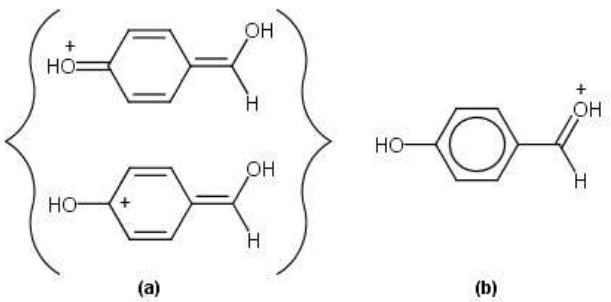

Figure 3. Conjugative interaction through the π-electron system between the *para* substituent and the protonated formyl group of ***p*-OH–BZH$^+$**.

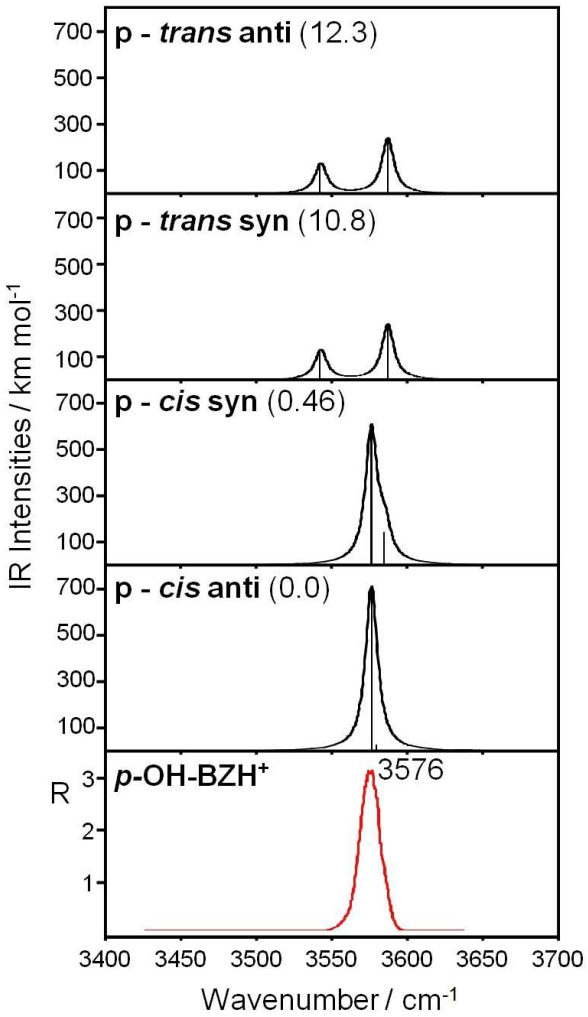

Figure 4. Experimental IRMPD spectrum of ***p*-OH–BZH$^+$** (bottom panel) recorded in the OH stretching range compared with the IR spectra computed for the low-energy isomers shown in Figure 2. Relative free energy values are given in parenthesis (kJ/mol).

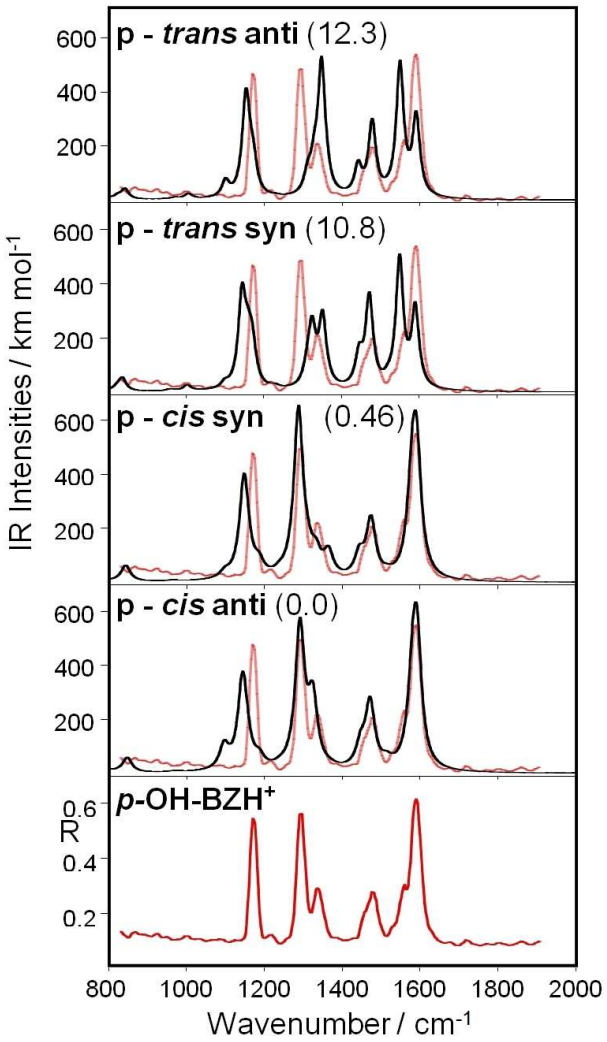

Figure 5. Experimental IRMPD spectrum of ***p*-OH–BZH$^+$** (bottom panel, red profile) in the fingerprint range compared with the IR spectra of the four isomeric structures shown in Figure 2. Relative free energy values are given in parenthesis (kJ/mol).

the experimental spectrum (Figure S3) confirming that protonation exclusively occurs at the formyl oxygen atom.

To confirm the evidence obtained in the O–H stretching range, the IRMPD spectrum of ***p*-OH–BZH$^+$** was recorded also in the fingerprint range and is compared in Figure 5 with the calculated spectra of the four isomeric ions. In this spectral range, two photofragments are detected when the laser frequency is resonant with an active vibrational mode of ***p*-OH–BZH$^+$** (Figure S4). The major one is the *m/z* 95 photofragment already observed. The second product ion at *m/z* 77 corresponds to the phenyl cation and involves also loss of water. The experimental IRMPD spectrum of ***p*-OH–BZH$^+$** recorded between 800 and 2000 cm^{-1} exhibits five main features at 1173, 1293, 1340, 1476, and 1590 cm^{-1} (Figure 5). Comparison between the calculated and experimental spectra supports once again the presence of **p-*cis*** isomers only. Thus, the vibrational modes of ***p*-OH–BZH$^+$** can be assigned as described in Table 1, which lists the experimental IRMPD features together with the calculated IR bands of the global minimum **p-*cis* anti**. Focusing on the two vibrational modes involving mainly the protonated formyl group in the fingerprint range, namely the CO_{fo} and the $C_{ar}C_{fo}$ stretching modes (fo = formyl, ar = aromatic), those related to **p-*cis*** conformers computed at 1291 and 1581 cm^{-1} are well matched in the IRMPD spectrum by the bands at 1293 and 1590 cm^{-1}, respectively.

In the computed spectra of the **p-*trans*** isomers, these two modes are predicted at around 1350 and 1550 cm^{-1} respectively and do not seem to contribute significantly to the experimental spectrum.

Thus, the fingerprint IRMPD spectrum of ***p*-OH–BZH$^+$** validates the conclusions drawn from the O–H stretching range, regarding a largely overwhelming presence of **p-*cis*** isomers.

Table 1. Positions of the IRMPD bands of protonated *para*-hydroxybenzaldehyde (***p*-OH–BZH$^+$**) and computed vibrational modes for the lowest-energy **p-*cis* anti** isomer.

Wavenumber [cm^{-1}] IRMPD	Calculated[a]	Vibrational mode[b]
Fingerprint range		
–	846 (55)	β_CH$_{ar}$ oop
1173	1096 (86)	β_CH$_{ar}$ ip
	1143 (316)	β_OH$_{ph}$ ip
	1152 (59)	β_CH$_{ar}$ ip
	1186 (36)	β_OH$_{fo}$ ip
1293	1291 (527)	σ_CO$_{fo}$ + β_CH$_{fo}$ ip
1340	1324 (240)	σ_CO$_{ph}$ + β_CH$_{ar}$ ip
1476	1447 (79)	σ_CC$_{ar}$
	1471 (245)	β_CH$_{ar}$ ip + σ_CC$_{ar}$ + σ_CO$_{ph}$
1590	1581 (269)	σ_C$_{ar}$C$_{fo}$
	1592 (447)	σ_CC$_{ar}$ (ring breathing)
OH stretch range		
3576	3576 (696)	(σ_OH$_{fo}$ + σ_OH$_{ph}$)$_{as}$
	3580 (26)	(σ_OH$_{fo}$ + σ_OH$_{ph}$)$_{s}$

[a] Vibrational frequencies calculated at the B3LYP/6-311++G(2df2p) level of theory. The computed intensities (km/mol) are given in parenthesis. In the fingerprint range, bands with intensity lower than 30 km/mol are not reported. [b] β = bending; σ = stretching; oop = out-of-plane; ip = in-plane; ar = aromatic; ph = phenolic; fo = formyl; as = antisymmetric; s = symmetric.

2.3. Protonated *m*-Hydroxybenzaldehyde

The next step was to ascertain whether the proximity of the hydroxyl group could affect the protonation on the formyl oxygen. To this end, protonated *m*-hydroxybenzaldehyde (***m*-OH–BZH$^+$**) was investigated by IRMPD in both the OH stretching and fingerprint range. Considering the possible geometries, it is important to note that for both *ortho* and *meta* hydroxybenzaldehydes two additional rotamers are possible for each configuration, yielding a larger number of structures relative to the *para* isomer. These new rotamers depend on the relative position of the protonated carbonyl oxygen with respect to the ring hydroxyl substituent that can be placed on the same or opposite side of the aromatic ring, named **a** or **b**, respectively. The optimized geometries of the eight carbonyl protonated *m*-hydroxybenzaldehyde ions (and their relative energies) are reported in Figure 6. Once again, *cis* conformations are more stable than the corresponding *trans*, but in this case the energetic disparity between *cis*/*trans* conformers is smaller. The most stable *trans* rotamer, **m-*trans* syn a** is only 3.6 kJ/mol higher in energy than the least stable *cis* one **m-*cis* anti b**, which in turn lies 4.0 kJ/mol above the global minimum **m-*cis* anti a**. However, the energy barrier for *cis/trans* interconversion is 58.0 kJ/mol, as calculated for the **m-*cis* anti a** to **m-*trans* syn a** path (see Figure S5 reporting the PES for interconversion paths between selected geometries of ***m*-OH–BZH$^+$**), midway between the corresponding barriers for

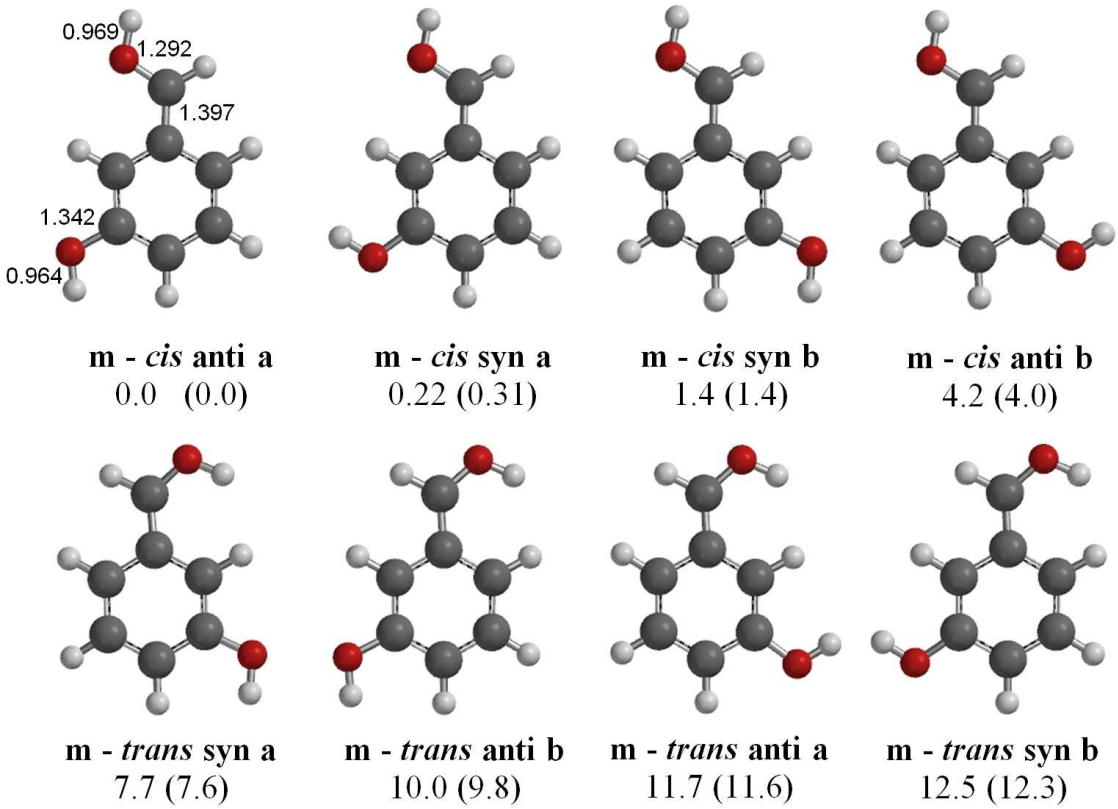

Figure 6. Optimized geometries for ***m*-OH–BZH$^+$**. Relative enthalpy and free energy (in parentheses) values (kJ/mol) at 298 K are computed at the B3LYP/6-311++G(2df2p) level.

BZH$^+$ and ***p*-OH–BZH$^+$**. Due to the electronic effects of the formyl and OH substituents, one may reasonably exclude protonation on the aromatic ring. Another possible protonation site in ***m*-OH–BZH$^+$**, namely the phenol oxygen, was considered. However, the most stable oxonium ion is 123.9 kJ/mol higher in energy than the global minimum (Figure S6).

The IRMPD spectrum of ***m*-OH–BZH$^+$** recorded between 3400 and 3700 cm^{-1} is compared in Figure 7 to the spectra calculated for the ions depicted in Figure 6. The experimental spectrum of ***m*-OH–BZH$^+$** shows two features at 3551 and 3620 cm^{-1} that fit well with the calculated spectra of the four *cis* conformers, for which the absorptions for the OH_{fo} and OH_{ph} stretching modes are calculated to be within ± 2 cm^{-1} around 3553 and 3618 cm^{-1}, respectively. In the computed spectra of the four *trans* conformers, the OH_{ph} stretching mode occurs, as expected, at nearly the same position as calculated for the *cis* isomers, namely around 3617 cm^{-1}, whereas the frequency of the OH_{fo} stretching mode is calculated to be ca. 3511 cm^{-1} for **m-*trans* syn b**, **m-*trans* syn a** and **m-*trans* anti b**, and 3523 cm^{-1} for **m-*trans* anti a**. The observed red shift conforms to the similar finding in the calculated spectra of *cis/trans* ***p*-OH–BZH$^+$** isomers. The search for any feature at this lower wavenumber (e.g., by using long irradiation time) failed, confirming once again that protonation yields only *cis* carboxonium conformers. Protonation at the phenolic oxygen atom can be excluded because the characteristic symmetric and antisymmetric stretching modes of the OH_2^+ moiety, predicted at 3451 and 3528 cm^{-1}, respectively, are missing in the experimental spectrum of ***m*-OH–BZH$^+$** as reported in Figure S6. This result is not unexpected in view of the high energy of this isomer.

Significantly, the experimental O–H stretching frequencies of ***m*-OH–BZH$^+$** and ***p*-OH–BZH$^+$** reveal the extent of the conjugative interaction through the π-electron system as a function of the position of the substituent. Previous experimental and theoretical studies have illustrated that protonation of benzaldehyde renders the formyl group more electron-withdrawing, without, however, completely destroying the π character of the C–O bond.[8] Consequently, in ***p*-OH–BZH$^+$**, protonation at the formyl oxygen enhances the electron-releasing property of the phenolic OH group, thus increasing its resonance contribution. The result is a contraction of both the C_{ar}–C_{fo} and C_{ar}–O_{ph} bonds and an elongation of the C–O_{fo} bond (Figure 3a). In ***m*-OH–BZH$^+$**, the resonance contribution is not as efficient and the charge stabilization effect is smaller, as reported for other *meta*-substituted benzaldehydes protonated in solution.[8b] As shown in Figure S7, where the calculated bond lengths of the global minimum conformers of *m*-, ***p*-OH–BZH$^+$** are depicted and compared with those of protonated phenol and BZH$^+$, in ***p*-OH–BZH$^+$**, the O–H_{fo} bond is shorter while O–H_{ph} bond is longer compared to ***m*-OH–BZH$^+$**, an effect that may be related to the extent to which the respective oxygen atom is involved in π-conjugation. When this participation is more pronounced, as in the *para* O_{ph} relative to *meta*, the increased length and diminished energy of the O–H_{ph} bond reduce the frequency of this stretching mode. The observed values are 3576 and 3620 cm^{-1} for ***p*-OH–BZH$^+$** and ***m*-OH–BZH$^+$**, respectively (consistent with O–H_{ph} bond lengths of 0.967 and 0.964 Å calculated for **p-*cis* anti** and **m-*cis* anti a**, respectively, as reported in Figures 2, 6 and S7). As expected, the opposite behavior is observed for the OH_{fo} stretching frequency, occurring at 3576 cm^{-1} for ***p*-OH–BZH$^+$** and at 3551 cm^{-1} for ***m*-OH–BZH$^+$** [once again compatible with O–H_{fo} bond lengths of 0.967 and 0.969 Å calculated for **p-*cis* anti** and **m-*cis* anti a**, respectively (Figure S7)]. A similar behavior was observed in the IRMPD spectrum of the nominal biradical UV dissociation product of diiodotyrosine, where the phenol OH stretch was redshifted at 3600 cm^{-1}, coherent with the π

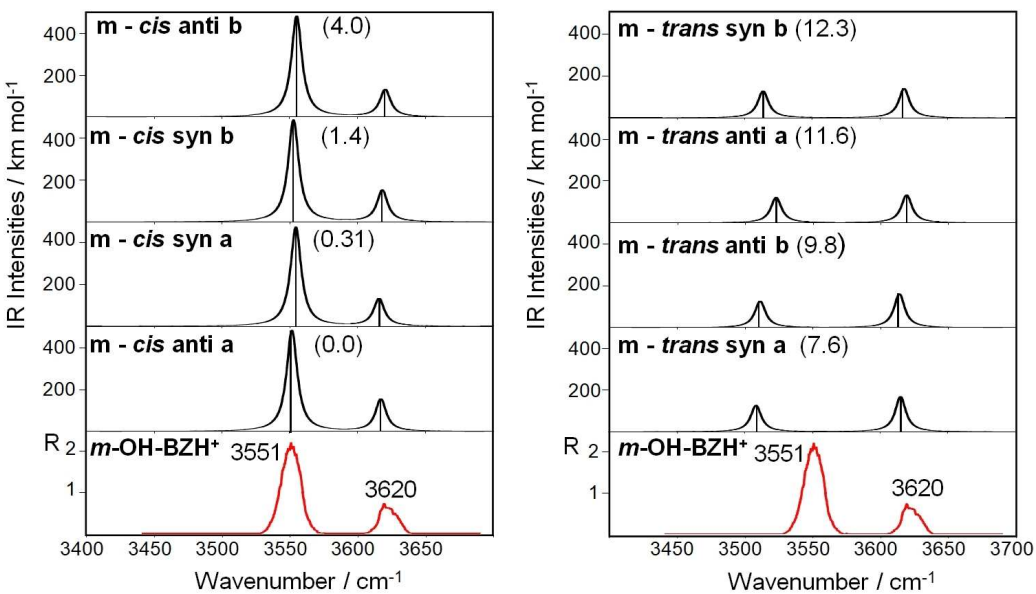

Figure 7. Experimental IRMPD spectrum of ***m*-OH–BZH$^+$** (bottom panel, in red) recorded in the OH stretching range compared to the IR spectra of the isomers shown in Figure 6. Relative free energy values are given in parenthesis (kJ/mol).

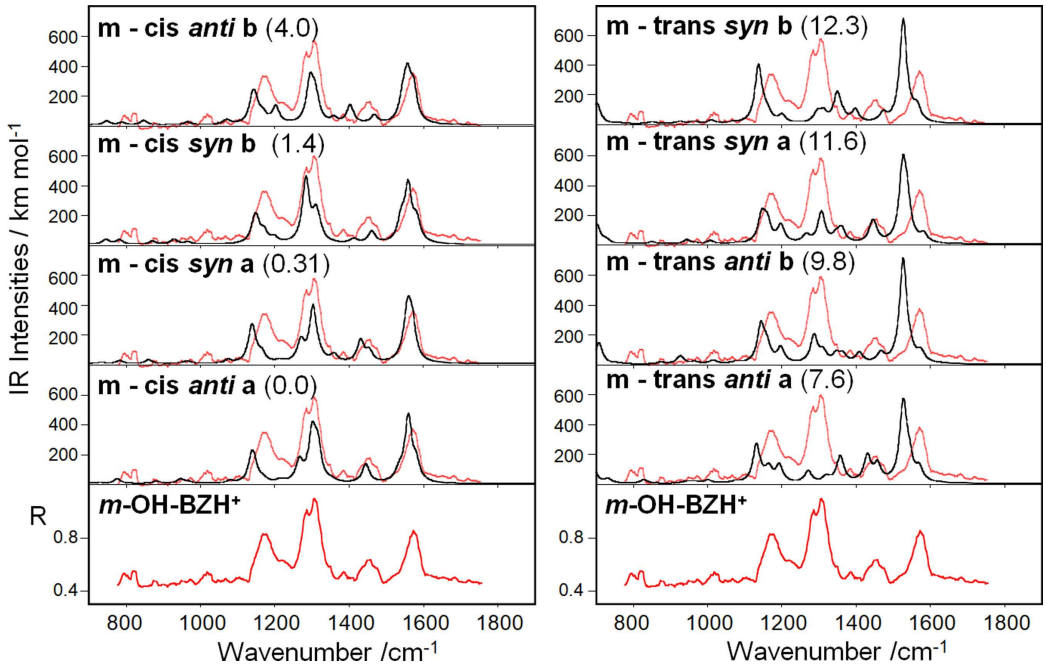

Figure 8. Experimental IRMPD spectrum of ***m*-OH–BZH$^+$** (bottom panel, red profile) in the fingerprint range compared with the IR spectra of the eight isomeric structures shown in Figure 6.

electron cloud completely delocalized over the whole molecule.[17]

To corroborate these evidences, the IRMPD spectrum of ***m*-OH–BZH$^+$** was also recorded in the fingerprint range, in order to compare the C–O stretching vibrations in the protonated *para*- and *meta*-hydroxybenzaldehydes and relate them to the efficiency of the π-electron delocalization.

The spectrum is reported in Figure 8, together with the calculated spectra of the eight more stable isomers in the ***m*-OH–BZH$^+$** series. It appears clearly that the experimental spectrum fits perfectly with those of *cis* conformers. So, as reported in Table 2, the vibrational modes of ***m*-OH–BZH$^+$** can be assigned with reference to the calculated IR bands of the global minimum **m-*cis* anti a**.

Focusing on the C–O stretching vibrations, the experimental CO_{fo} vibration of ***m*-OH–BZH$^+$** can be attributed to the experimental band at 1306 cm^{-1} as highlighted in Figure 9, and reported in Table S1. This same vibrational mode is found at 1293 cm^{-1} in the experimental spectrum of ***p*-OH–BZH$^+$** (Table S1). This redshift suggests that the C–O bond of the protonated formyl group presents a more pronounced single bond character in the ***p*-OH–BZH$^+$** isomer with respect to ***m*-OH–BZH$^+$**, in agreement with calculated bond lengths of 1.302 and 1.292 Å for **p-*cis* anti** and **m-*cis* anti a**, respectively.

Furthermore, the experimental $C_{ar}C_{fo}$ stretching mode, observed at 1576 and 1590 cm^{-1} for ***m*-OH–BZH$^+$** and ***p*-OH–BZH$^+$**, respectively, reveals a greater double bound character in the *para* isomer (calculated bond length of 1.384 Å versus 1.394 Å for the *meta* isomer). As reported in Table S1, it is interesting to note that these two experimental (and theoretical) absorptions of the *meta* isomer are very similar to the ones reported for **BZH$^+$**.[13] Indeed, the calculated bond lengths of the protonated formyl group of ***cis* BZH$^+$** and **m-*cis* anti a** are essentially identical, as reported in Figure S7.

Concentrating on the CO_{ph} stretching mode (Figure 9), it occurs at 1286 cm^{-1} in the IRMPD spectrum of the ***m*-OH–BZH$^+$**. Contrary to the behavior displayed by the CO_{fo} stretching, this mode is blue-shifted in the spectrum of the ***p*-OH–BZH$^+$**, and appears at 1340 and 1476 cm^{-1}. In the latter

Table 2. Positions of the IRMPD bands of protonated *meta*-hydroxybenzaldehyde (***m*-OH–BZH$^+$**) and computed vibrational modes for the lowest-energy **m-*cis* anti a** isomer.

Wavenumber [cm^{-1}] IRMPD Fingerprint range	Calculated[a]	Vibrational mode[b]
1166	1138 (177)	$\beta\_OH_{ph}+\beta\_CH_{ar}$
	1146 (63)	$\beta\_CH_{ar}+\beta\_OH_{ph}$
1226	1214 (17)	$\beta\_OH_{fo}+\beta\_CH_{fo}$
1286	1266 (137)	$\sigma\_CO_{ph}+\beta\_CH_{ar}$
1306	1300 (316)	$\beta\_CH_{ar}+\beta\_CH_{fo}$
	1315 (228)	$\sigma\_CO_{fo}+\beta\_CH_{ar}$
	1471 (245)	$\beta\_CH_{ar}+\sigma\_CC_{ar}$
1453	1445 (107)	$\sigma\_CC_{ar}+\beta\_CH_{ar}$
1576	1534 (69)	σ_CC_{ar}
	1559 (438)	$\sigma\_C_{ar}C_{fo}$
	1580 (114)	σ_CC_{ar}
OH stretch range		
3551	3552 (484)	σ_OH_{fo}
3620	3618 (155)	σ_OH_{ph}

[a] Vibrational frequencies calculated at the B3LYP/6-311++G(2df2p) level of theory. The computed intensities (km/mol) are given in parenthesis. In the fingerprint range, bands with intensity lower than 30 km/mol are not reported. [b] β = bending; σ = stretching; ar = aromatic; ph = phenolic; fo = formyl.

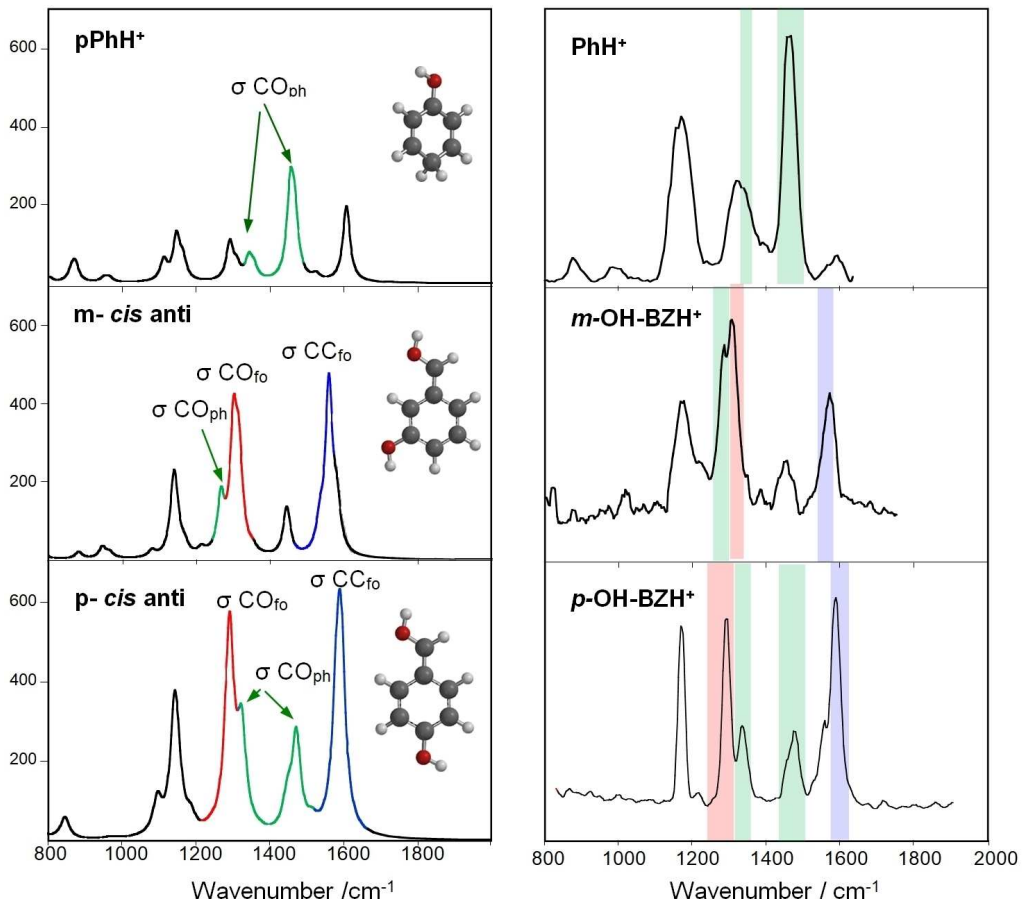

Figure 9. Comparison between experimental (right side) and calculated (left side) IR(MPD) spectra of ***p*-OH–BZH$^+$**, ***m*-OH–BZH$^+$** and protonated phenol (**PhH$^+$**) in the fingerprint range.

feature the CO_{ph} stretching is coupled with the $C_{ar}C_{ar}$ stretching. Therefore, the C–O_{ph} bond shows an enhanced double-bond character in protonated *para*-hydroxybenzaldehyde relative to the *meta* isomer.

Overall, the observed frequencies point to an electronic configuration shifted almost completely towards structure (**b**) for the *meta* isomer and structures (**a**) for the *para* isomer as shown in Figure 3, thus validating the interpretation based on vibrational spectroscopy in the OH stretching range.

2.4. Protonated Phenol Assayed as Reference Species

To complete the picture, the IRMPD spectrum of protonated phenol was recorded in the fingerprint range, in order to gain independent experimental information about the C–O_{ph} stretching vibration of this reference aromatic compound. Protonated phenol has in fact never been yet assayed in the fingerprint range by IR action spectroscopy. The IRMPD spectrum of protonated phenol, **PhH$^+$** is presented in Figure 10 (blue trace, bottom panel) and compared with the calculated spectra for all possible isomers, already illustrated in previous studies reporting the IRPD spectrum in the O–H stretching range.[2a,c,e]

The visual inspection shows a best fit with the spectrum computed for the global minimum, namely the *para* protonated isomer, ***p*-PhH$^+$**, in agreement with previous evidence pointing to predominant protonation at the para position.[2a,c,e,18] Vibrational modes can be assigned as described in Table 3, which lists the experimental IRMPD absorptions together with the calculated IR transitions of the ***p*-PhH$^+$**. The CO_{ph} stretching mode of **PhH$^+$** is assigned to the experimental features at 1343 and 1462 cm^{-1}, that occur at nearly the same frequency observed for ***p*-OH–BZH$^+$** (Figure 9, Table S1). This finding provides further support for the extensive π-delocalization in ***p*-OH–BZH$^+$**, in spite of the charge being formally placed on a position external to the ring.

The IRMPD spectrum of protonated phenol has also provided an appropriate reference to gain structural information about the ion at *m/z* 95 formed by both CID and photofragmentation of ***p*-OH–BZH$^+$**. The IRMPD spectrum of the fragment ion is characterized by quite comparable features as the ones recorded for **PhH$^+$** (Figure S8 in the Supporting Information). The fragmentation product can be thus assigned the structure of *para* protonated phenol.

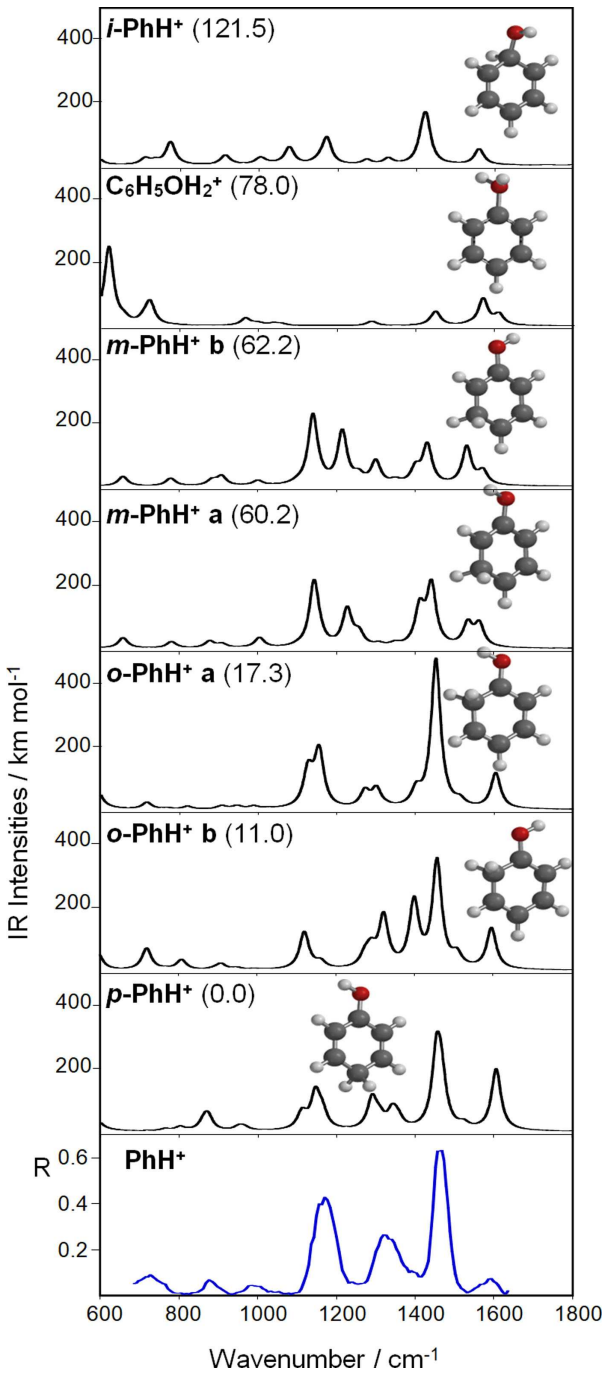

Figure 10. Experimental IRMPD spectrum **PhH$^+$** (bottom panel, blue trace) in the 700–1600 cm^{-1} range, compared with the IR spectra of **PhH$^+$** isomers. The optimized geometries are computed at the B3LYP/6-311++G(2df2p) level. Relative free energy at 298 K (in parentheses) values are in kJ/mol.

Table 3. IRMPD bands of protonated phenol and vibrational modes computed for the ***p*-PhH$^+$** isomer.

Wavenumber [cm^{-1}] IRMPD	Calculated[a]	Vibrational mode[b]
726	719 (68)[c]	rock_CH_2 + β_CH oop
881	862 (27)	σ_C_mC_o
	872 (47)	rock_CH_2 + β_CH oop
993	950 (12)	σ_C_mC_o
	964 (12)	wag_CH_2
1180	1112 (53)	β_CH ip
	1146 (112)	β_OH ip + β_C_oH ip
	1164 (48)	β_CH ip (o,m sciss type)
1322	1291 (97)	sciss CH_2
	1310 (32)	β_CH ip
	1342 (54)	σ_CO + β_CH ip (o,m)
	1356 (31)	β_CH ip + σ_CC
1462	1455 (222)	σ_CC
	1467 (138)	σ_CC + σ_CO
1600	1606 (194)	σ_CC (ring breathing)

[a] Vibrational modes calculated at the B3LYP/6-311++G**(2df2p) level of theory. The computed intensities (km/mol) are given in parentheses. [b] β = bending; σ = stretching; rock = rocking; wag = wagging; sciss = scissoring; ip = in-plane; oop = out-of-plane; o = *ortho*, m = *meta*. [c] vibrational modes computed for the ***o*-PhH b**.

2.5. Protonated *o*-Hydroxybenzaldehyde

As last though more complex species, protonated *o*-hydroxybenzaldehyde has been assayed to understand if and how the orientation of proton attachment could be influenced by an OH group in *ortho* position. Due to the proximity of the two substituents in *o*-hydroxybenzaldehyde, the possibility of forming an intramolecular H-bond between the phenolic and protonated carbonyl groups may play an important role, as observed by NMR studies on protonated *o*-fluorobenzaldehyde.[8b] Moreover considering the directing nature of the two substituents in electrophilic aromatic substitution, protonation at the ring can also occur in *meta* position with respect to the carbonyl, which is at the same time *para* (or *ortho*) relative to the hydroxyl group. Figure 11 reports the optimized geometries of the seven conformers for the carboxonium ion together with the most stable ring carbenium ion (*para*-protonated with respect to the hydroxyl substituent). In contrast with previous findings for the *meta* isomer, there are only seven, instead of eight, possible stable structures protonated at the carbonyl group. In fact, the hypothetic **o-*trans* anti a** does not converge to a minimum, due to strong repulsion between the two O-bound hydrogen atoms facing each other. For the first time, the global minimum has a *trans* configuration, corresponding to **o-*trans* syn a**, stabilized by an intramolecular H-bond between the oxygen atom of the hydroxyl group and the hydrogen atom of protonated formyl.

Moreover, once again at variance with the behaviour of ***p*-OH–BZH$^+$** and ***m*-OH–BZH$^+$**, the *cis* conformers are not all close in energy. The most stable *cis* conformer, **o-*cis* syn b**, lies 9.7 kJ/mol above the global minimum, while the least stable one, **o-*cis* anti b**, is located at 37.7 kJ/mol. The **o-*cis* syn a** is worth a comment. The energy of this isomer is rather high relative to the global minimum in spite of a geometrical arrangement that may suggest the presence of a H-bond between the phenol hydrogen and the former formyl oxygen. Actually, bond distances are rather different. The O–H bond lengths of the phenol and protonated formyl group are 0.967 and 0.968 Å, respectively, in **o-*cis* syn a** and 0.968 and 0.981 Å in **o-*trans* syn a**. The putative H-bond distance separating the phenol hydrogen atom from the former formyl oxygen in **o-*cis***

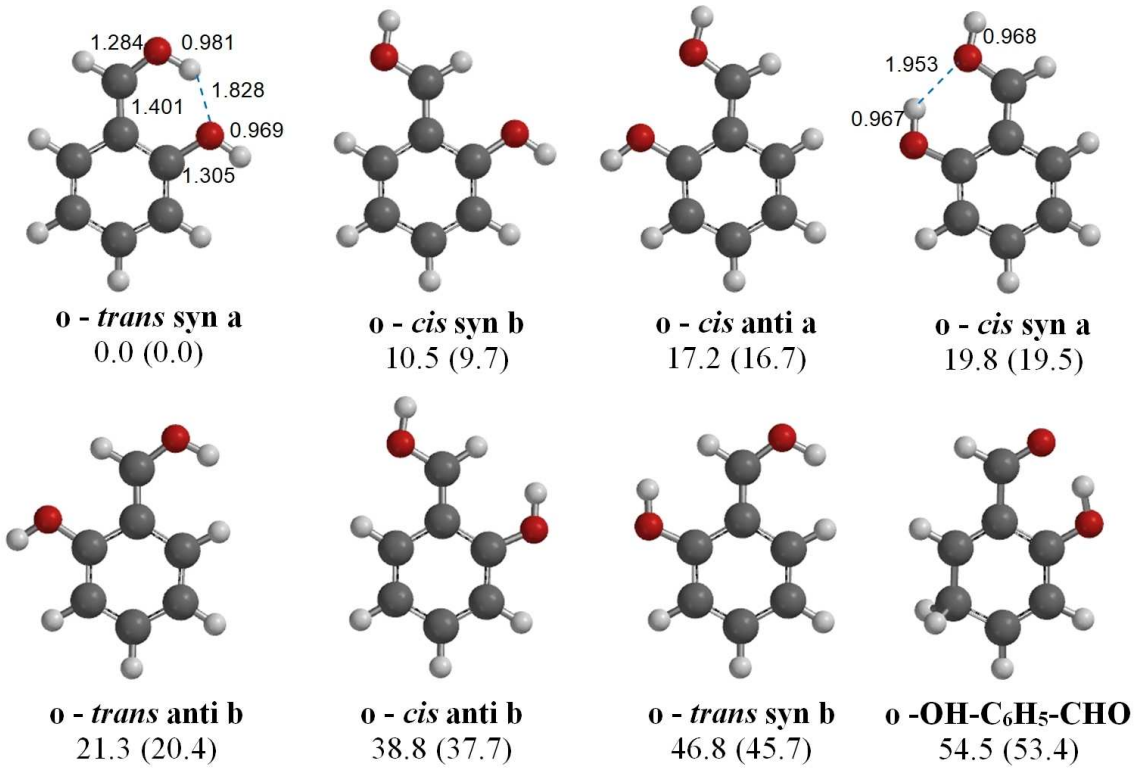

Figure 11. Optimized geometries for ***o*-OH–BZH$^+$** in either carboxonium or ring carbenium configuration. Relative enthalpy and free energy (in parentheses) values (kJ/mol) at 298 K are computed at the B3LYP/6-311 + +G(2df2p) level.

syn a is equal to 1.953 Å, a much larger value relative to 1.828 Å separating the carboxyl hydrogen atom from the phenol oxygen in **o-*trans* syn a**. There is clearly a tiny H-bond interaction within **o-*cis* syn a**. This finding may be accounted for by the positively polarized carboxyl oxygen in **o-*cis* syn a** making it a poor H-bond acceptor.

The most stable carbenium isomer, ***o*-OH–C$_6$H$_5$–CHO** is only 53.4 kJ/mol higher in energy relative to the global minimum. Here again we note a difference relative to both ***p*-OH–BZH$^+$** and **BZH$^+$**, for which the most stable ring carbenium ion is more than 100 kJ/mol above the global minimum. Additionally, the energy barrier of 69.5 kJ/mol for the interconversion from **o-*trans* syn a** to **o-*cis* anti a** is the highest in the series of the examined hydroxybenzaldehydes, as depicted in Figure S9 where the PES of the interconversion path between the three most stable carboxonium isomers of ***o*-OH–BZH$^+$** is reported. Despite the presence of an electron-donor substituent in *ortho* position, which should decrease the double-bond character of C–O$_{fo}$, as observed for ***p*-OH–BZH$^+$**, the H-bond between the proton on the formyl group and the oxygen atom of the hydroxyl group inhibits the rotation around the C–O$_{fo}$ bond. On the other hand, considering that **o-*cis* anti a** lies at 16.7 kJ/mol above the global minimum, the activation energy for the back isomerization process is 52.7 kJ/mol, similar to the one calculated for ***p*-OH–BZH$^+$**.

The energy ordering of the calculated structures accounts well for the IRMPD spectrum of ***o*-OH–BZH$^+$** recorded between 3200 and 3700 cm^{-1} and reported in Figure 12, along with the spectra calculated for the structures shown in Figure 11. There are three absorptions in the IRMPD spectrum of ***o*-OH–BZH$^+$**. The major one at 3590 cm^{-1} exhibits a shoulder at 3585 cm^{-1}, a minor one appears at 3557 cm^{-1} and a broad one is comprised between 3310 and 3410 cm^{-1}. Three different features for only two O–H bonds suggest that at least two different isomers are present in the sample. Comparing the experimental spectrum with the calculated ones in Figure 10, one may exclude any contribution of the higher energy isomers, specifically **o-*trans* syn b**, **o-*cis* anti b**, and **o-*trans* anti b**. These three species have predicted absorptions that do not match with any band in the experimental spectrum (see Table S2, where the stretching frequencies of the OH$_{ph}$ and OH$_{fo}$ bonds are reported for all calculated structures). The spectrum of the global minimum **o-*trans* syn a** shows two absorptions at 3340 and 3587 cm^{-1}, attributed to the stretching of OH$_{fo}$ involved in the H-bond with the phenolic oxygen atom and the free OH$_{ph}$ bond, respectively, which can account for most of the experimental signals, namely the broad band at 3310–3410 cm^{-1}, and the main feature at 3590 cm^{-1}. The broad shape of the band at 3310–3410 cm^{-1} can be justified by noting that X–H stretching modes (X=N,O) involved in H-bonding are reported to display unexpectedly low intensity when the photofragmentation process requires more than one photon to reach the fragmentation threshold and most frequently appear as broad rather than sharp absorptions.[3,19] Together with a major fraction of **o-*trans* syn a**, another possible rotamer contributing to the observed IRMPD spectrum is **o-*cis* anti a**, although it lies at 16.8 and 7.0 kJ/mol

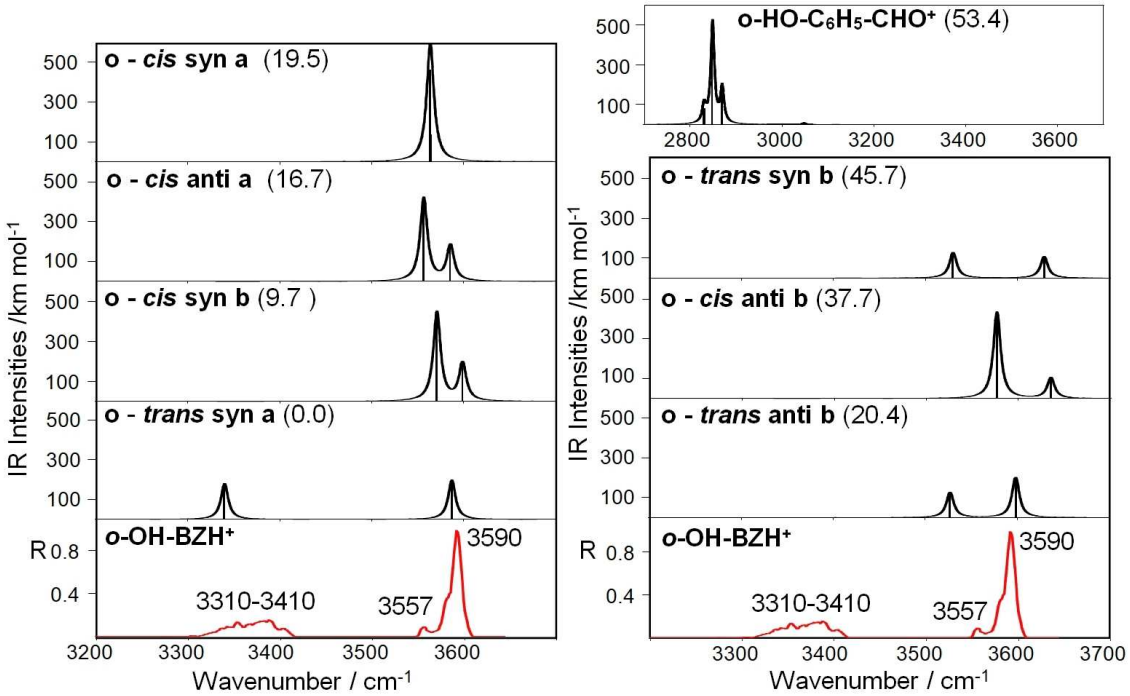

Figure 12. Experimental IRMPD spectrum of ***o*-OH–BZH$^+$** (bottom panel, in red) recorded in the OH stretching range compared to the IR spectra of the optimized isomers presented in Figure 11. Relative free energy values are given in parenthesis (kJ/mol).

above the global minimum and its more stable rotamer **o-*cis* syn b**, respectively. The small experimental band at 3557 cm^{-1}, and the shoulder observed at 3585 cm^{-1}, match with the calculated spectrum of **o-*cis* anti a**, and correspond to the OH_{fo} and OH_{ph} stretching modes predicted at the same frequencies. A minor contribution of other comparably stable isomers, **o-*cis* syn b** and **o-*cis* syn a**, to the sampled ***o*-OH–BZH$^+$** ions cannot be discarded.

In the current interpretation, a less stable rotamer, such as **o-*cis* anti a**, is contributing to the ionic population. A kinetic bias towards its formation may however be traced to the fact that, as already noticed for ***m/p*-OH–BZH$^+$**, the *cis* conformation of the protonated formyl group does not suffer from steric hindrance by the adjacent phenyl group. The high barrier for rearrangement into **o-*trans* syn a** may justify the significant contribution of **o-*cis* anti a** in the sampled population.

3. Conclusions

Structural isomers of **OH–BZH$^+$** formed in solution, delivered by ESI and isolated in the gas phase, were characterized by IRMPD spectroscopy and quantum chemical calculations. It was demonstrated that protonation of ***m/p*-OH–BZH$^+$** occurs only at the formyl oxygen atom to generate carboxonium ions of exclusively *cis* conformation. Moreover, the experimental O–H and C–O stretching frequency are indicative of a significant conjugative interaction through the π-electron system in ***p*-OH–BZH$^+$** when compared to ***m*-OH–BZH$^+$**. Only in the case of the ***o*-OH–BZH$^+$** isomer, in addition to the two more stable conformers with *cis* configuration, the presence of one isomer with *trans* configuration, stabilized by intramolecular H-bonding between the oxygen atom of the phenolic OH group and the hydrogen atom delivered onto the formyl group, was observed. The occurrence of a *trans* conformer in the sampled ***o*-OH–BZH$^+$**, largely favored thermodynamically, may yet suffer from a kinetic bias towards formation of the *cis* carboxonium ion.

Experimental Section

Ion Production

Benzaldehyde and *ortho*, *meta*, and *para*-hydroxybenzaldehydes were research grade products from commercial sources (Sigma-Aldrich s.r.l. Milan, Italy) used without further purification. Protonated (hydroxy)benzaldehyde isomers were obtained as gaseous ions in an electrospray ionization source (ESI) by infusion of a hydro-alcoholic solution of the selected compounds (10^{-5} M in MeOH/H_2O 2/1 with 2% acetic acid) by way of a syringe pump. Typical ESI conditions were a flow rate of 180 μl/h, a spray voltage of 4500 V and a capillary temperature of 230 °C. Nebulizer gas was set at 15 PSI and drying gas flow at 5 L/min. Mass analysis showed abundant ions corresponding to protonated benzaldehyde (*m/z* 106.9), or protonated *o, m,* or *p*-hydroxybenzaldehydes (*m/z* 122.8), according to the injected solution.

In a different experiment, protonated phenol was obtained by chemical ionisation of phenol in a mobile FT-ICR mass spectrometer analyser (MICRA)[20] using $C_2H_5^+$ as protonating agent. $C_2H_5^+$ ions

were generated by chemical ionization using CH_4 as reagent gas. Details of the procedure are available in Ref [9d].

IRMPD Experiments

Two distinct energy ranges were considered for IRMPD experiments. Vibrational modes associated with the OH stretches were investigated by recording IRMPD spectra in the 3200–3700 cm^{-1} frequency range. For this purpose, an optical parametric oscillator/amplifier (OPO/OPA) (LaserVision) coupled to a Paul ion trap mass spectrometer (Esquire 6000+, Bruker Daltonics), was employed as described previously.[21] The typical output energy from the OPO/A laser (3–4 cm^{-1} bandwidth) was 25–30 mJ/pulse. In the trap, ions were accumulated for 30 ms and then mass-selected prior to IR irradiation. Post-irradiation mass spectra were recorded averaging 5 accumulations. The irradiation time was varied from 0.3 to 2 s depending on the system. The laser frequency was calibrated by comparing atmospheric water absorptions along the IR laser path to published data.[22] To confirm evidences obtained in the higher frequency range, the IRMPD spectrum of protonated *para*-hydroxybenzaldehyde was also recorded in the fingerprint range (800–2000 cm^{-1}) using the beamline of the free electron laser (FEL) at the Centre Laser Infrarouge d'Orsay (CLIO). For the present study, the electron energy of the FEL was set at 44 MeV, to optimize the laser power in the frequency range of interest. The FEL beamline is coupled with a hybrid FT-ICR tandem mass spectrometer (APEX–Qe Bruker) equipped with a 7.0 T actively shielded magnet and a quadrupole-hexapole interface for mass-filtering and ion accumulation, under control of the commercial software APEX 1.0. Mass-selection of the ion under study was performed in the quadrupole and ions were accumulated in the hexapole containing argon buffer gas for 0.5 s for collisional cooling prior to their transfer into the ICR cell. The isolated parent ions were then irradiated for 500 ms with the IR FEL light, after which the resulting ions were mass-analyzed.[23] IRMPD spectra were obtained by plotting the photofragmentation yield R ($R = -\ln[I_{parent}/(I_{parent} + \Sigma I_{fragment})]$, where I_{parent} and $I_{fragment}$ are the integrated intensities of the mass peaks of parent and fragment ions, respectively) as a function of the frequency of the IR radiation.[23] In a related experiment, the IRMPD spectrum of protonated phenol was measured by coupling a lab-built FT-ICR to CLIO.[9b,24] In these experiments, the electron energy of the FEL was set at 41 MeV to cover the spectral range 700–1650 cm^{-1}. The parent ions were irradiated for 1 s and 5 mass spectra were accumulated and averaged.

Computational Details

Density functional theory calculations were carried out using the B3LYP density functional,[25] as implemented in the Spartan 10 suite of programs. The different structures considered have been optimized using the 6–311++G(2df2p) basis set, without any symmetry constraint. Harmonic vibrational frequencies were determined at this same level to characterize the stationary points as local minima or saddle points, and to estimate the zero-point vibrational energy (ZPE) corrections. The linear infrared absorption spectra of the various structures were calculated within the harmonic approximation. A scaling factor of 0.949 was applied to the calculated frequencies in the 3200–3700 cm^{-1} range and of 0.960 in the fingerprint range, on the basis of the good agreement between experimental and scaled computed frequencies.[26] Finally, for consistency with the experimental spectral resolution, the calculated stick spectra were convoluted by Lorentzian line profiles using a full width at half maximum of 5 and 15 cm^{-1} in the OH stretch and fingerprint ranges, respectively.

Acknowledgements

This study was supported by Sapienza Università di Roma (prot. RP11715 C6456718F), the Italian Ministry for Education, University and Research – Dipartimenti di Eccellenza – L. 232/2016, Deutsche Forschungsgemeinschaft (DFG DO 729/3) and the European Commission (CLIO project IC17-002). The research leading to this result has been supported by the project CALIPSOplus under the Grant Agreement 730872 from the EU Framework Programme for Research and Innovation HORIZON 2020. Financial Support from the National FT-ICR network (FR3624 CNRS) for conducting the research is gratefully acknowledged. We thank N. Solcà for assistance in recording the IRMPD spectrum of PhH^+ and we are grateful to J. M. Ortega, D. Scuderi, J. Lemaire, and the technical support at the CLIO facility.

Conflict of Interest

The authors declare no conflict of interest.

Keywords: aromatic aldehydes · IR action spectroscopy · mass spectrometry · oxonium ion · phenol

[1] a) D. M. Brouwer, E. L. Mackor, C. MacLean, in *Carbonium Ions* Vol II (Eds.: G. A. Olah, P. v. R. Schleyer), Wiley, New York, **1970**; b) M. B. Smith, J. March, in *Advanced Organic Chemistry. Reactions, Mechanisms, and Structure*, 5th ed.; Wiley: New York, **2001**, Chapter 11; c) G. A. Olah, *Acc. Chem. Res.* **1971**, *4*, 240–248; d) B. Chiavarino, M. E. Crestoni, C. H. DePuy, S. Fornarini, R. Gareyev, *J. Phys. Chem.* **1996**, *100*, 16201–16208.

[2] a) N. Solcà, O. Dopfer, *Chem. Phys. Lett.* **2001**, *342*, 191–199; b) N. Solcà, O. Dopfer, *Angew. Chem. Int. Ed.* **2003**, *42*, 1537–1540; c) N. Solcà, O. Dopfer, *J. Am. Chem. Soc.* **2004**, *126*, 1716–1725; d) F. M. Pasker, N. Solcà, O. Dopfer, *J. Phys. Chem.* **2006**, *110*, 12793–12804; e) M. Katada, A. Fujii, *J. Phys. Chem. A* **2018**, *122*, 5822–5831.

[3] a) B. Chiavarino, M. E. Crestoni, M. Schütz, A. Bouchet, S. Piccirillo, V. Steinmetz, O. Dopfer, S. Fornarini, *J. Phys. Chem. A* **2014**, *118*, 7130–7138; b) A. Bouchet, M. Schütz, B. Chiavarino, M. E. Crestoni, S. Fornarini, O. Dopfer, *Phys. Chem. Chem. Phys.* **2015**, *17*, 25742–25754; c) M. Schütz, A. Bouchet, B. Chiavarino, M. E. Crestoni, S. Fornarini, O. Dopfer, *Chem. Eur. J.* **2016**, *22*, 8124–8136; d) J. Oomens, G. von Helden, G. Meijer, *J. Phys. Chem. A* **2004**, *108*, 8273–8278.

[4] a) G. Culberton, R. Pettit, *J. Am. Chem. Soc.* **1963**, *85*, 741–743; b) K. Yates, R. Stewart, *Can. J. Chem.* **1959**, *37*, 664–671; c) J.-F. Gal, S. Geribaldi, G. Pfister-Guillouzo, D. G. Morris, *J. Chem. Soc. Perkin Trans. 2* **1985**, *1*, 103–106; d) D. Stuart, S. D. Wetmore, M. Gerken, *Angew. Chem. Int. Ed.* **2017**, *56*, 16380–16384.

[5] G. A. Olah, K. K. Laali, Q. Wang, G. K. S. Prakash, in *Onium Ions*, Wiley, New York, **1998**, p. 269–34.

[6] H. Meerwein, in *Methoden der Organischen Chemie* (Eds.: E. Müller), Houben-Weyl 4th Ed., Vol 6/3, Thieme, Stuttgart, **1965**.

[7] S. R. Miller, S. Krasutsky, P. Kiprof, *J. Mol. Struct.* **2004**, *674*, 43–47.

[8] a) R. Jost, P. Rimmelin, J. M. Sommer, *J. Chem. Soc. D*, **1971**, 879–881; b) R. Jost, J. M. Sommer, T. Drakenberg, *Org. Magn. Reson.* **1975**, *7*, 351–354; c) A. Halouia, E. Halouia, *J. Phys. Org. Chem.* **2014**, *27*, 430–439.

[9] a) N. Solcà, O. Dopfer, *Angew. Chem. Int. Ed.*, **2002**, *41*, 3628–3631; b) W. Jones, P. Boissel, B. Chiavarino, M. E. Crestoni, S. Fornarini, J. Lemaire, P. Maitre, *Angew. Chem. Int. Ed.* **2003**, *42*, 2057–2059; c) N. Solcà, O. Dopfer, *J. Am. Chem. Soc.* **2003**, *125*, 1421–1430; d) O. Dopfer, N. Solcà, J. Lemaire, P. Maître, M. E. Crestoni, S. Fornarini, *J. Phys. Chem. A* **2005**, *109*, 7881–7887; e) B. Chiavarino, M. E. Crestoni, S. Fornarini, J. Lemaire, L. MacAleese, P. Maitre, *ChemPhysChem* **2005**, *6*, 437–440; f) J. Oomens, B. G. Sartakov, G. Meijer, G. von Helden, *Int. J. Mass Spectrom.* **2006**, *254*, 1–19; g) O. Dopfer, J. Lemaire, P. Maître, B. Chiavarino, M. E. Crestoni, S. Fornarini, *Int. J. Mass Spectrom.* **2006**, *249–250*, 149–154 ; h) O. Dopfer, *J. Phys. Org. Chem.* **2006**, *19*, 540–551; i) U. J. Lorenz, N. Solcà, J. Lemaire,

P. Maître, O. Dopfer, *Angew. Chem. Int. Ed.* **2007**, *46*, 6714–6716; j) B. Chiavarino, M. E. Crestoni, O. Dopfer, P. Maitre, S. Fornarini, *Angew. Chem. Int. Ed.* **2012**, *51*, 4947–4949.
[10] a) X. Yi, H. Q. Gu, Q. Q. Gao, Z. L. Liu, J. Bao, *Biotechnol. Biofuels* **2015**, *8*, 153; b) S. Larsson, A. Quintana-Sainz, A. Reimann, N. O. Nilvebrant L J Jonsson, *Appl. Biochem. Biotechnol.* **2000**, *84–86*, 617–632.
[11] D. Cao, M. Tu, R. Xie, J. Li, Y. Wu, S. Adhikari, *J. Agric. Food Chem.* **2014**, *62*, 918–926.
[12] R. Xie, M. Tu, T. Elder, *Energy Fuels* **2016**, *30*, 3078–3084.
[13] B. Chiavarino, M. E. Crestoni, S. Fornarini, O. Dopfer, J. Lemaire, P. Maître, *J. Phys. Chem. A* **2006**, *110*, 9352–9360.
[14] a) S. Chakraborty, A. Patzer, O. Dopfer, *J. Chem. Phys.* **2010**, *133*, 044307; b) O. Dopfer, A. Patzer, S. Chakraborty, I. Alata, R. Omidyan, M. Broquier, C. Dedonder, C. Jouvet, *J. Chem. Phys.* **2014**, *140*, 124314.
[15] a) I. Alata, R. Omidyan, C. Dedonder-Lardeux, M. Broquier, C. Jouvet, *Phys. Chem. Chem. Phys.* **2009**, *11*, 11479–11486; b) A. Patzer, M. Zimmermann, I. Alata, C. Jouvet, O. Dopfer, *J. Phys. Chem. A* **2010**, *114*, 12600–12604.
[16] G. A. Olah, G. Rasul, C. York, G. K. S. Prakash, *J. Am. Chem. Soc.* **1995**, *117*, 11211–11214.
[17] K. Ranka, N. Zhao, L. Yu, J. F. Stanton, N. C. Polfer, *J. Am. Soc. Mass Spectrom.* **2018**, *29*, 1791–1801.
[18] N. Solcà, O. Dopfer, *J. Chem. Phys.* **2004**, *120*, 10470–10482.
[19] a) M. Broquier, F. Lahmani, A. Zehnacker-Rentien, V. Brenner, P. Millié, A. Peremans, *J. Phys. Chem. A* **2001**, *105*, 6841–6850; b) K. Mackeprang, H. G. Kjaergaard, T. Salmi, V. Hänninen, L. Halonen, *J. Chem. Phys.* **2014**, *140*, 184309 ; c) J. M. Bakker, R. K. Sinha, T. Besson, M. Brugnara, P. Tosi, J. Y. Salpin, P. Maitre, *J. Phys. Chem. A* **2008**, *112*, 12393–12400; d) B. Chiavarino, M. E. Crestoni, S. Fornarini, D. Scuderi, J.-Y. Salpin, *Inorg. Chem.* **2017**, *56*, 8793–8801; e) A. F. DeBlase, S. Bloom, T. Lectka, K. D. Jordan, A. B. McCoy, M. A. Johnson, *J. Chem. Phys.* **2013**, *139*, 024301; f) A. Kamariotis, O. V. Boyarkin, S. R. Mercier, R. D. Beck, M. F. Bush, E. R. Williams, T. R. Rizzo, *J. Am. Chem. Soc.* **2006**, *128*, 905–916; g) H. U. Ung, K. T. Huynh, J. C. Poutsma, J. Oomens, G. Berden, T. H. Morton, *Int. J. Mass Spectrom.* **2015**, *378*, 294–302; h) X. Li, J. Oomens, J. R. Eyler, D. T. Moore, S. S. Iyengar, *J. Chem. Phys.* **2010**, *132*, 244301.
[20] G. Mauclaire, J. Lemaire, P. Boissel, G. Bellec, M. Heninger, *Eur. J. Mass Spectrom.* **2004**, *10*, 155–162.
[21] a) A. De Petris, A. Ciavardini, C. Coletti, N. Re, B. Chiavarino, M. E. Crestoni, S. Fornarini, *J. Phys. Chem. Lett.* **2013**, *4*, 3631–3635; b) M. E. Crestoni, B. Chiavarino, D. Scuderi, A. Di Marzio, S. Fornarini, *J. Phys. Chem. B* **2012**, *116*, 8771–8779; c) B. Chiavarino, M. E. Crestoni, S. Fornarini, S. Taioli, I. Mancini, P. Tosi, *J. Chem. Phys.* **2012**, *137*, 024307.
[22] C. Camy-Peyret, J. M. Flaud, G. Guelachvili, C. Amiot, *Mol. Phys.* **1973**, *26*, 825–855.
[23] a) J. Lemaire, P. Boissel, M. Heninger, G. Mauclaire, G. Bellec, H. Mestdagh, A. Simon, S. Le Caer, J. M. Ortega, F. Glotin, P. Maitre, *Phys. Rev. Lett.* **2002**, *89*, 273002–1; b) J. M. Bakker, T. Besson, J. Lemaire, D. Scuderi, P. Maitre, *J. Phys. Chem. A* **2007**, *111*, 13415–13424.
[24] G. Mauclaire, J. Lemaire, P. Boissel, G. Bellec, M. Heninger, *Eur. J. Mass Spectrom.* **2004**, *10*, 155–162.
[25] a) C. Lee, W. Yang, R. G. Parr, *Phys. Rev. B* **1988**, *37*, 785–789; b) A. D. Becke, *J. Chem. Phys.* **1993**, *98*, 5648–5652.
[26] a) I. M. Alecu, J. Zheng, Y. Zhao, D. G. Truhlar, *J. Chem. Theory Comput.* **2010**, *6*, 2872–2887; b) J. Zheng, I. M. Alecu, B. J. Lynch, Y. Zhao, D. G. Truhlar, https://comp.chem.umn.edu/freqscale/version2.htm, **2010**.

Manuscript received: January 15, 2020
Accepted manuscript online: January 17, 2020
Version of record online: ■■, ■■■

ARTICLES

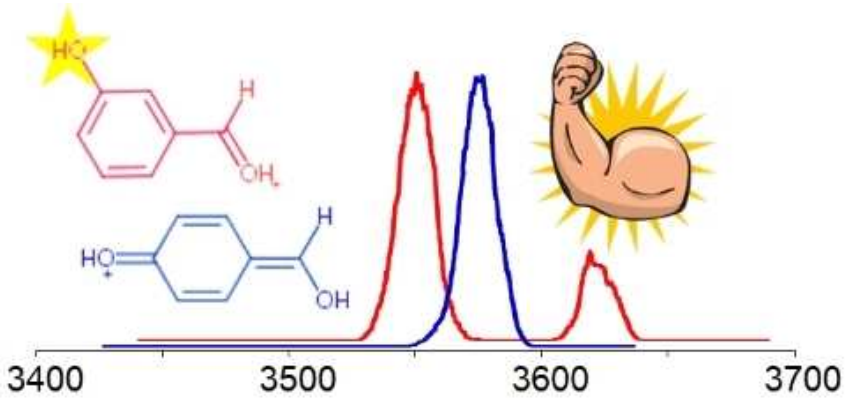

Showing strengths: O–H stretching frequencies of protonated ***p*-hydroxybenzaldehyde** and ***m*-hydroxybenzaldehyde** prove to be a sensitive indicator of the strength of conjugative interaction between substituents through the π-electron system.